This is a pre-print of the article:

Pegueroles-Queralt, J., F. D. Bianchi, and O. Gomis-Bellmunt. "A power smoothing system based on supercapacitors for renewable distributed generation". *IEEE Transactions on Industrial Electronics*, In press, 2014.

DOI: 10.1109/TIE.2014.2327554

IEEEXplore Digital Library: http://ieeexplore.ieee.org/xpl/articleDetails.jsp?arnumber=6823757

A power smoothing system based on supercapacitors for renewable distributed generation

Jordi Pegueroles-Queralt, Fernando D. Bianchi and Oriol Gomis-Bellmunt *Senior Member, IEEE*

***Abstract*—With the increasing share of renewable power sources in distributions networks, a smooth delivery of the power generated has become a relevant requirement for ensuring proper power quality. This article presents a simple power smoothing strategy based on supercapacitors for power conditioning of distributed renewable generation. The power smoothing controller generates the power reference for the DC/DC converter which has a power tracking control implemented with sliding mode techniques. The proposed strategy consists on a voltage controller capable of maintaining the optimal state of charge and reducing high frequency components of the power coming from renewable energy sources. A generalization of the PI structure is used to ensure simple design and implementation. With the proposed control structure, the tuning is reduced to find a state feedback gain based on a pole placement criterion. In addition, a criterion for selecting supercapacitors' size is provided. The effectiveness of the proposed power smoothing scheme is evaluated by simulations and validated in an experimental platform.**

***Index Terms*—Energy storage systems, microgrids, power electronics, power smoothing, supercapacitors.**

I. Introduction

THE introduction of dispersed renewable generation sources in the distribution network has been growing in the last decade. Renewable distributed generation impacts on power systems in a number of ways, with special relevance the variability of the electrical production. The penetration of distributed generation may result in degradation of the power quality, especially in the case of weak networks [1], [2] or microgrids [3]. Fast fluctuation of power generation produces voltage oscillations (flicker), with frequency range between 1 and 10 Hz [4]. Its effects can vary from electric disturbances to epileptic attacks in photosensitive persons. Flicker may also affect sensitive electronic systems, such as telecommunication equipment or industrial processes, relying on high quality power supply [5].

A possible approach to diminish voltage fluctuations produced by converter-based generation,in weak networks and microgrids, is to actively damp the specific frequency by only employing the capacitance of the DC-link [6]. However, the smoothing of a wider range of frequencies requires the use of energy storage systems (ESSs). Several storage technologies are available for smoothing purposes [7]. In particular, supercapacitors are an emerging technology specially suitable in cases demanding fast charge and discharge cycles, such as the power smoothing in renewable energy applications [8]. Storage systems for power smoothing present different interfaces with the grid. In the case of individual renewable power sources interfaced with a full power back-to-back power converter, it is common to attach the energy storage system to the DC-link [9]–[14]. In other cases, the energy storage system is equipped with its own inverter, permitting its association with one or more sources simultaneously, or its integration in a microgrid. Commonly, the ESS is connected at the point of common coupling of the renewable source, see *e.g.* [15]–[18].

In power smoothing, a compromise must be reached between the attenuation of the fast variation in power and the regulation of the state of charge. This last objective is necessary to maximize the capability of absorbing and delivering energy, ensuring a good power smoothing. Commonly, to achieve these objectives, two control laws are used yielding to schemes that might be difficult to design [11], [15], [17], [19]. For example, the integration of supercapacitors in a doubly fed induction generator to reduce the fast wind-induced power variations is considered in [11]. The proposed fuzzy logic based energy management system is used to set the power set-point of the wind turbine combined with storage in order to optimize the overall operation of the system. The energy manager uses the predicted wind power production, energy storage device status and history, and AC voltage measurements. Kamel et al. propose to combine pitch control of wind power and ESS based on supercapacitors for smoothing power fluctuations in microgrid applications [16]. A filter extracts the mean wind power, which is used as the power reference for the system wind turbine with storage. The supercapacitor system compensates the power mismatch between the computed average power reference and the actual wind power, leaving the state of charge unconstrained. The problem of finding the correct size of the supercapacitor bank tied to the output of a direct wave energy converter to ensure a smooth power profile is analyzed in [12]. In this application the ESS power setpoint is the result of a fuzzy rule combining both the difference between a constant grid power reference and the actual produced power, and the state of charge of the ESS. A different approach is presented by Jayasinghe and Vilathgamuwa [20], where clamped supercapacitors are used, in the DC-link of a three-level voltage source converter, to

J. Pegueroles-Queralt, F. D. Bianchi and O. Gomis-Bellmunt are with the Catalonia Institute for Energy Research, IREC, Jardins de les Dones de Negre 1, 08930 Sant Adrià de Besòs (Barcelona), Spain. O. Gomis-Bellmunt is also with the Centre d'Innovació Tecnològica en Convertidors Estàtics i Accionaments (CITCEA-UPC) Universitat Politècnica de Catalunya, Av. Diagonal 647, Pl. 2, 08028 Barcelona, Spain

The research of J. Pegueroles-Queralt, F.D. Bianchi and O. Gomis-Bellmunt was supported by the European Regional Development Funds (ERDF, "FEDER Programa Competitivitat de Catalunya 2007-2013") and by the European union seventh framework program FP7 - SMARTCITIES - 2013 IDEAL project, under grant aggreement 608860.

remove the fast fluctuations in wind power applications. The smoothing is accomplished by the inertia introduced by the supercapacitors in the converter.

In this article, in contrast with the previous approaches of power tracking problems, the power smoothing is expressed as a filtering problem. With this approach, the power smoothing consists in attenuating the high frequency components of the power delivered by the renewable source. Then, the power smoother results in a rather simple voltage control scheme, which permits to specify the cut-off smoothing frequency, while guaranteeing optimal state of charge of the storage system, without the requirement of additional filters or prediction algorithms. The proposed control design helps to find a trade-off between state of charge regulation and smoothing capability. The power smoothing system is connected directly to the AC grid to obtain a flexible implementation for smoothing different variable power sources. Guidelines to determine the size of the storage element according to the cut-off frequency and power levels of the application are also provided. The power smoothing scheme has been implemented in a supercapacitor based ESS to smooth wind power. This application has been evaluated by simulations and experiment in a laboratory environment.

II. Power smoothing with supercapacitors

Consider an aggregation of renewable sources injecting a fast varying power P_{ren} into the grid. The idea of power smoothing is to generate a power profile P_{ESS} to compensate the fast varying components of P_{ren} and to produce a slow varying power output $(P_{out} = P_{ren} + P_{ESS})$ delivered to the low voltage grid or microgrid. In other words, power smoothing consists in attenuating the components of P_{out} for frequencies greater than a boundary value ω^d, *i.e.*

$$|P_{out}(j\omega)| < \epsilon, \qquad \forall\, \omega > \omega^d, \tag{1}$$

where ω is the frequency and ϵ is a small arbitrary value. If the objective of the power smoothing would be to suppress flicker, the value ω^d should be in the range of frequencies of the voltage oscillations (1 to 10 Hz).

The topology adopted in this article to reduce the variability in the electric production of an aggregation renewable sources is sketched in Fig. 1. The constructive details of the energy storage block ESS can be found in [21]. The ESS is interfaced with the rest of the network through a grid side converter (GSC) controlled by K_{GSC}, which regulates the voltage V_{DC} maintaining energy balance in the DC-link. The controller of the energy storage side converter (ESSC), K_{ESSC}, regulates the power exchanged between the energy storage device (ESD) and the DC-link. Fig. 2 presents the bidirectional DC/DC topology adopted to implement the ESSC. In this application, the voltage V_{DC} (on the left side) is always higher than V_{ESD} (on the right side), but energy can flow in both directions. This converter can work in buck mode delivering energy to the storage device or in boost mode draining energy from the storage device.

As the DC-link provides a certain degree of decoupling between ESSC and GSC, the design of each controller can be

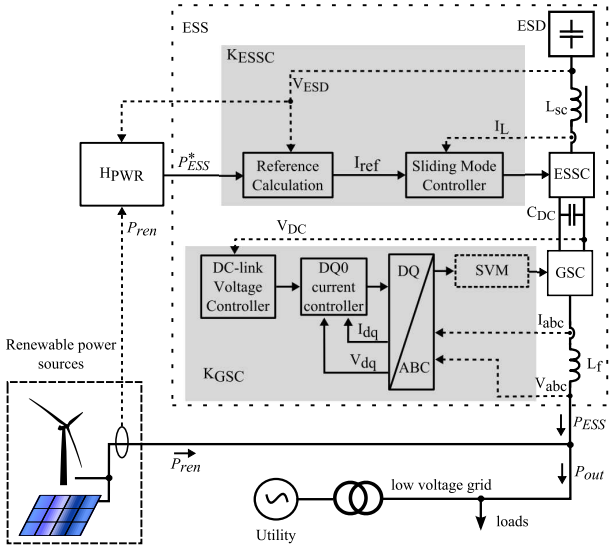

Fig. 1. Layout of the power smoothing system

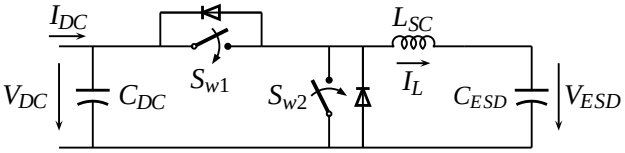

Fig. 2. Bidirectional DC-DC topology used in the ESSC

independent. Usually, the GSC is controlled with a cascaded control scheme. For details on the control of the GSC, see e.g. [22], [23]. The DC/DC controller K_{ESSC} is implemented using sliding mode techniques. A single sliding surface, which is used as the switching law, is shaped dynamically to achieve one of the three operating modes: pre-charge, power tracking or voltage limitation. More details on the ESSC design can be found in [21].

For power smoothing analysis, the supercapacitors can be assumed pre-charged and in power tracking operation. In this state, ESS can absorb or deliver power to the grid tracking a power reference P^*_{ESS}. In power tracking mode, the dynamics of the ESS can be described by

$$G_{ESS}: \begin{cases} \dot{V}_{ESD} = \dfrac{P^*_{ESS}}{V_{ESD} C_{ESD}}, \\ \dot{P}_{ESS} = \dfrac{P^*_{ESS} - P_{ESS}}{\tau_{GSC}}, \end{cases} \tag{2}$$

where P^*_{ESS} is the power reference for the ESS, V_{ESD} and C_{ESD} are the supercapacitors' voltage and capacity respectively, and τ_{GSC} is the time constant of the GSC.

The voltage of the supercapacitor bank must be constrained in the operating range

$$V_{ESD_{min}} < V_{ESD} < V_{ESD_{max}}, \tag{3}$$

as high current could arise if voltage V_{ESD} decreases to small values and an upper limit must be imposed to preserve the integrity of the supercapacitors. The control developed in [21] ensures the voltage remains inside these limits under all possible operating conditions.

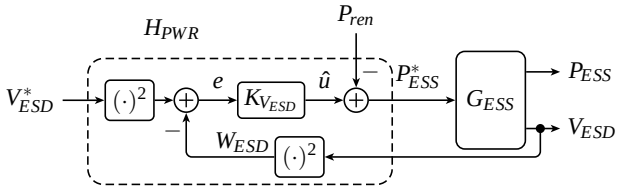

Fig. 3. Structure of the proposed power smoothing controller H_{PWR}

The state of charge SoC of the ESD is defined as

$$SoC = \frac{V_{ESD}^2 - V_{ESD_{min}}^2}{V_{ESD_{max}}^2 - V_{ESD_{min}}^2}. \tag{4}$$

Maintaining a 50 % SoC is important to maximize smoothing capability of the ESS. A low value of SoC limits the system to deliver the necessary energy to the grid. Otherwise, an ESS with a high SoC could not be able to absorb the amount energy needed for power smoothing.

III. Proposed power smoothing strategy

The main component of the power smoothing system is the controller H_{PWR}. In Fig. 1, the power smoothing controller H_{PWR} produces a power reference P^*_{ESS}, the setpoint for ESS, by measuring the total output power from renewable sources P_{ren} and monitoring the SoC of ESS. In order to guarantee a long term operation, the power smoothing controller must ensure that the SoC of ESD is at 50 % in average. This prevents the voltage from reaching the saturation limits ensuring a better capability to absorb or deliver power in any situation.

The proposed structure for the power smoothing controller H_{PWR} is shown in Fig. 3, where G_{ESS} are the dynamics described in (2). The core of H_{PWR} is the voltage controller $K_{V_{ESD}}$ producing a control signal $\hat{u}$ with its bandwidth limited to ω_c. The power reference P^*_{ESS} sent to the ESS is the power P_{ren} delivered by the renewable energy source subtracted from $\hat{u}$. The voltage controller $K_{V_{ESD}}$ must be designed to maintain V_{ESD} close to the reference V^*_{ESD} in low frequencies (see III-A) to ensure a proper SoC of the supercapacitors. Simultaneously, the controller H_{PWR} must also produce a high frequency signal P_{ESS} capable of attenuating P_{ren} for frequencies above ω^d, *i.e.*

$$|P_{ren}(j\omega) + P_{ESS}(j\omega)| < \epsilon, \qquad \forall\, \omega \geq \omega^d \geq \omega_c, \tag{5}$$

where ω_c is the bandwidth of the power smoothing control.

Clearly, the key point to achieve these objectives is the design of the voltage controller $K_{V_{ESD}}$ and the correct selection of the supercapacitors capacity. These points are analyzed in detail in the following subsections.

A. ESS sizing

Taking into account voltage limits of the supercapacitors and current limits of the converter, it is important to select the most suitable storage device for achieving the best power smoothing at lower cost. In this subsection, a selection criterion is proposed based on a worst case scenario.

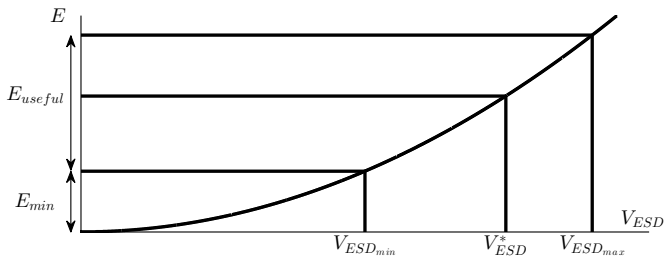

Fig. 4. Relation between the supercapacitors voltage V_{ESD} and the energy stored

The energy that the supercapacitor can absorb or deliver for smoothing purposes is given by

$$E_{useful} = \frac{1}{2} C_{ESD} V_{ESD_{max}}^2 - E_{min}, \tag{6}$$

where $E_{min} = \frac{1}{2} C_{ESD} V_{ESD_{min}}^2$ denotes the energy required to raise the voltage up to $V_{ESD_{min}}$, *i.e.* E_{min} is the amount of energy not used due to the lower voltage limit. To have the largest possible amount of energy available for smoothing purposes, the voltage reference V^*_{ESD} is selected as the value corresponding to 50 % of the SoC, *i.e.*

$$V^*_{ESD} = \sqrt{\frac{V_{ESD_{max}}^2 + V_{ESD_{min}}^2}{2}}. \tag{7}$$

These values of energy and voltage are illustrated in Fig. 4.

Considering the previous analysis, the following criteria can be used to determine the capacity of the energy storage element. First, it must be decided the cut-off frequency ω_c based on the particular needs of the application. Then, in the worst case scenario, the filtering element would have to generate a power

$$P_{ESS} = P_{ESD} \sin(\omega_c t). \tag{8}$$

That is, the disturbance to attenuate is a pure sinusoidal signal of maximum power, with P_{ESD} the nominal power of the ESS. In order to be able to completely cancel this signal, the ESD must store or inject the energy

$$E_{WC} = P_{ESD} \int_0^{\frac{\pi}{\omega_c}} \sin(\omega_c \tau) d\tau = 2\frac{P_{ESD}}{\omega_c} \tag{9}$$

If the supercapacitor voltage is maintained at V^*_{ESD}, the energy stored is $E_{useful}/2 + E_{min}$ (50 % of its capacity). Thus, to guarantee an energy level of E_{WC} available for power smoothing, supercapacitor must be sized such that

$$E_{useful} = 2E_{WC}. \tag{10}$$

Therefore, from (6),

$$C_{ESD} = \frac{4E_{WC}}{V_{ESD_{max}}^2 - V_{ESD_{min}}^2}. \tag{11}$$

Notice that this criterion is based on the assumption of perfect filtering, therefore the lower frequency to be generated by the smoother is ω_c. In practice, this is not completely true since other frequencies will be present. However, this approximation provides a useful guideline to select the capacity of the storage device.

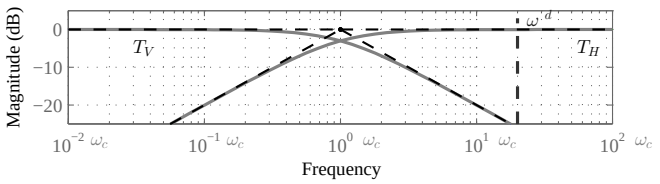

Fig. 5. Desirable asymptotic frequency responses of the transfer functions $T_H(s)$ and $T_V(s)$

B. Design of voltage regulator $K_{V_{ESD}}$

In order to design a simple voltage controller, equation (2) is linearized by the change of variable $W_{ESD} = V_{ESD}^2$. Thus, voltage dynamics is governed by

$$\dot{W}_{ESD} = \frac{2}{C_{ESD}} P^*_{ESS}, \tag{12}$$

with a control signal expressed as $P^*_{ESS} = \hat{u} - P_{ren}$, where $\hat{u}$ is the control law

$$\hat{u} = K_{V_{ESD}}(W^*_{ESD} - W_{ESD}), \tag{13}$$

with $W^*_{ESD} = {V^*_{ESD}}^2$. Finally the controlled signal W_{ESD} is given by

$$W_{ESD} = G_{eq}(s)(\hat{u} - P_{ren}), \tag{14}$$

where $G_{eq} = 2/sC_{ESD}$.

To design the power smoother, two transfer functions are of interest: $T_H(s)$ from P_{ren} to P_{ESS} and $T_V(s)$ from W^*_{ESD} to W_{ESD}. As shown in Fig. 3, these transfer functions result in

$$T_H(s) = \frac{P_{ESS}(s)}{P_{ren}(s)} = \frac{-G_2(s)}{1 + G_{eq}(s)K_{V_{ESD}}(s)}, \tag{15}$$

$$T_V(s) = \frac{W_{ESD}(s)}{W^*_{ESD}(s)} = \frac{G_{eq}(s)K_{V_{ESD}}(s)}{1 + G_{eq}(s)K_{V_{ESD}}(s),} \tag{16}$$

with

$$G_2(s) = \frac{P_{ESS(s)}}{P^*_{ESS}(s)} = \frac{1}{s\tau_{ESD} + 1}. \tag{17}$$

To fulfill the control objectives aforementioned, the frequency responses of these transfer functions should be as illustrated in Fig. 5. That is, $T_H(s)$ should be a high pass filter with a cut-off frequency ω_c, to reproduce in P_{ESS} the high frequency components of P_{ren}. On the other hand, $T_V(s)$ should be a low pass filter with at least one pole located in $s = 0$ to maintain the supercapacitor voltage close to V^*_{ESD} and guarantee a proper SoC. The proposed structure for the controller $K_{V_{ESD}}$ is shown in Figure 6, where K_i $(i = 1, \ldots, n+1)$ are scalar parameters to be designed. This structure is a generalization of the classical PI that allows a simple design of a n-order filter. The order dependents on the needed accuracy of the bandwidth limitation. As will be shown, the controller structure in Figure 6 reduces the design to the computation of a simple state feedback gain $K_{sf} = \begin{bmatrix} K_1 & K_2 & \ldots & K_n & K_{n+1} \end{bmatrix}$ to place the closed loop poles in a desired location.

Let $x_{K_{vi}}$ $(i = 1, \ldots, n)$ be the controller states, then the open loop system formed with the proposed controller

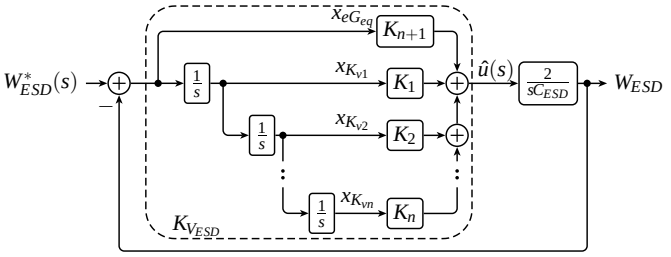

Fig. 6. General block diagram of the voltage controller $K_{V_{ESD}}$

structure and $G_{eq}(s)$ is given by

$$\dot{x} = \begin{bmatrix} A_{st} & \Upsilon \\ 0 & 0 \end{bmatrix} x + \begin{bmatrix} 0 & B_{st} \\ 2/C_{ESD} & 0 \end{bmatrix} \begin{bmatrix} \hat{u} \\ W^*_{ESD} \end{bmatrix}, \tag{18}$$

where

$$A_{st} = \begin{bmatrix} 0 & 0 & \cdots & 0 \\ 1 & 0 & \cdots & 0 \\ \vdots & \ddots & \ddots & \vdots \\ 0 & \cdots & 1 & 0 \end{bmatrix}, \quad \Upsilon = \begin{bmatrix} -1 \\ 0 \\ \vdots \\ 0 \end{bmatrix}, \quad B_{st} = \begin{bmatrix} 1 \\ 0 \\ \vdots \\ 0 \end{bmatrix},$$

and $x = \begin{bmatrix} x_{K_{v1}}, & \ldots, & x_{K_{vn}}, & W_{ESD} \end{bmatrix}^T$. In this scheme, the control signal is given by

$$\hat{u} = K_{sf} x. \tag{19}$$

This state feedback control law can be computed *e.g.* by solving a standard pole placement problem [24]. More precisely, the closed loop matrix is given by

$$A_{cl} = \begin{bmatrix} A_{st} & \Upsilon \\ 2\tilde{K}_{sf}/C_{ESD} & K_{n+1} \end{bmatrix},$$

where $\tilde{K}_{sf} = [K_1\ K_2\ \ldots\ K_n]$. Using a similarity transformation T, this closed loop matrix in the controllable realization results

$$A^c_{cl} = T^{-1} A_{cl} T = \begin{bmatrix} 0 & & I_n \\ K^c_1 & \ldots & K^c_{n+1} \end{bmatrix},$$

where $K^c_{sf} = [K^c_1\ K^c_2\ \ldots\ K^c_{n+1}] = K_{sf}T$. The characteristic polynomial of A^c_{cl} is given by

$$\det(sI_{n+1} - A^c_{cl}) = s^{n+1} + K^c_{n+1}s^n + \cdots + K^c_2 s + K^c_1. \tag{20}$$

If all closed loop poles are located in $s = -\omega_c$, the desired closed loop characteristic polynomial is

$$(s+\omega_c)^{n+1} = s^{n+1} + \alpha_1 s^n + \alpha_2 s^{n-1} + \cdots + \alpha_n s + \alpha_{n+1}. \tag{21}$$

By comparing (20) and (21), the state feedback results

$$K_{sf} = \begin{bmatrix} \alpha_{n+1} & \alpha_n & \ldots & \alpha_1 \end{bmatrix} T^{-1}. \tag{22}$$

The controller $K_{V_{ESD}}(s)$ can be obtained as

$$K_{V_{ESD}}(s) = \tilde{K}_{sf}(sI_n - A_{st})^{-1} B_{st} + K_{n+1}. \tag{23}$$

For example, for $n = 2$, the state feedback gain is $K_{sf} = \begin{bmatrix} 3\omega_c^2 C_{ESD}/2 & \omega_c^3 C_{ESD}/2 & 3\omega_c C_{ESD}/2 \end{bmatrix}$ and the voltage controller

$$K_{V_{ESD}} = \frac{3\omega_c C_{ESD}}{2} + \frac{3\omega_c^2 C_{ESD}}{2s} + \frac{\omega_c^3 C_{ESD}}{2s^2}. \tag{24}$$

Then, the closed loop transfer functions become

$$T_H(s) = \frac{s^3}{(s+\omega_c)^3(s\tau_{ESD}+1)}, \quad (25)$$

$$T_V(s) = \frac{3\omega_c s^2 + 3\omega_c^2 s + \omega_c^3}{(s+\omega_c)^3}. \quad (26)$$

Transfer functions (25) and (26) obey the requirement on frequency response shown in Fig. 5. It is also clear that the transition region of the two filters are overlapped. These regions are smaller when the order of the controller is higher, achieving a more accurate frequency filtering. However, the order of the controller increases the complexity of the implementation.

The controller must be discretized to be implemented in a digital platform, such as a digital signal processor. The state-space realization of the discrete version is then balanced and expressed in the modal canonical form to avoid quantification effects and numerical issues [25]. This is important especially in digital platforms with fixed-point arithmetic. The discrete implementation results then in

$$x(k+1) = x(k) + B_c(W^*_{ESD}(k) - W_{ESD}(k)), \quad (27)$$

$$\hat{u}(k) = C_c x(k) + d_c(W^*_{ESD}(k) - W_{ESD}(k)). \quad (28)$$

where $B_c = [b_1 \ \dots \ b_n]^T$ and $C_c = [c_1 \ \dots \ c_n]$.

C. Guidelines for selecting the power smoothing controller parameters

In the scheme previously presented, the cut-off frequency, the controller order, the energy storage capacity and rated power are parameters to be selected in accordance to the power level to be smoothed. In the sequel, some general guidelines are given to help to select these parameters.

- The cut-off frequency ω_c determines the bandwidth of the power smoother and can be selected arbitrarily lower than the desired smoothing frequency ω^d. The filter order n determines the steepness of the transition region. The higher the order the more accurate is the component cancellation in the power spectrum. Selecting ω_c close to ω^d can result in a high order controller, and low value of ω_c requires a high capacity of the ESS. The separation between ω_c and ω_d defines the magnitude of T_H at ω_d, see Fig. 5. With the pole placement given in (21) and assuming that $\omega_d \ll 1/\tau_{ESD}$,

$$|T_H(\omega_d)| \approx \left(\omega_c/\sqrt{\omega_d^2+\omega_c^2}\right)^{n+1}.$$

  Therefore, it is straightforward to prove that by setting the cross-frequency as

$$\omega_c = \sqrt{1-\varepsilon^{2/(n+1)}}\omega_d,$$

  the attenuation at ω_d is approximately ε. This formula can be used to select the suitable ω_c depending on the controller order.
- There is a trade-off between capacity of the ESS and smoothing capabilities. The higher the capacity C_{ESD}, the smoother the power output. High capacities also prevents reaching capacity limits; if the limits are reached, the filter is disabled until the voltage is restored to the operating range (3), either by charging or discharging supercapacitors.
- The energy storage rated power P_{ESD} is given by the power converter limits and typically is chosen between $10-40$ % of the rated power of renewable energy source [26].

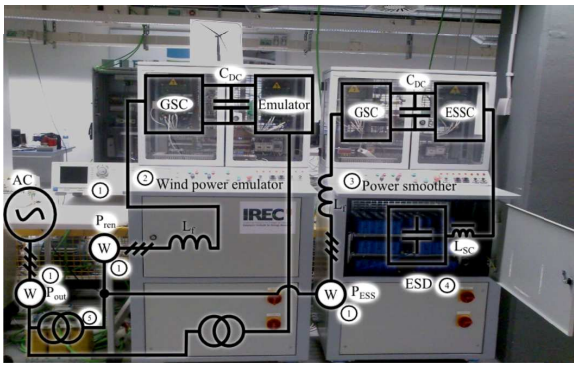

Fig. 7. Experimental setup for the implementation of the power smoothing controller. Set-up includes: 1, power meter; 2, wind turbine emulator; 3, power smoother cabinet; 4 , supercapacitor bank; 5, transformer at the point of common coupling.

IV. Case study: Wind power smoothing

To illustrate the design of the proposed scheme, the technique is used to smooth the power injected into the grid by a wind turbine of 373 kW. The smoothing controller is evaluated by simulation and experiment (in a scaled version).

The experimental setup is shown in Fig. 7, which emulates the smoothing scheme in Fig. 1. The objective is to reduce the power oscillations injected by the wind turbine. Basically, the experimental setup consists of two back-to-back converter, with a DC-link voltage of 650 V, connected to a 400 V AC grid through an isolating transformer. One power converter emulates the power profile of a wind turbine of 373 kW. The other converter implements the power smoother proposed in this article. The storage device of the power smoothing system is a supercapacitor bank of 400 V_{DC}, 4 kW and 60 Wh, with $V_{ESD_{min}} = 250\ V$ and $V_{ESD_{max}} = 450\ V$. For more details on the hardware of the experimental setup see [21]. It is worth mentioning that due to hardware limitations on the available equipment to emulate the wind turbine [27], the power ratings in the experimental set-up are lower than the ratings used in simulation case.

The power injected by the wind turbine emulator presents the typical short-term spectrum shown in Fig. 8. This spectrum was obtained from the model presented in [28], [29] taking into account the studies carried out by Thringer and Dahlberg [30]. The wind profile corresponds to a mean wind speed of 8 m/s and a turbulence intensity of 18 %. The turbulence intensity quantifies the variability of wind speed within 10 minutes. The wind turbine rated power is 373 kW, and the rated wind speed is about 11 m/s. It can be observed in the spectrum in Fig. 8 that the wind power presents a prominent component close to 1.1 Hz, which is transferred to the grid as a power ripple of several kW.

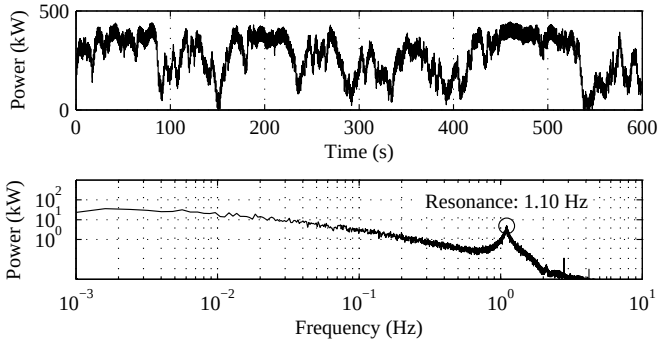

Fig. 8. Profile of P_{ren}, the signal emulating the power injected by a 375 kW wind turbine with mean wind speed of 8 m/s, and the corresponding spectrum

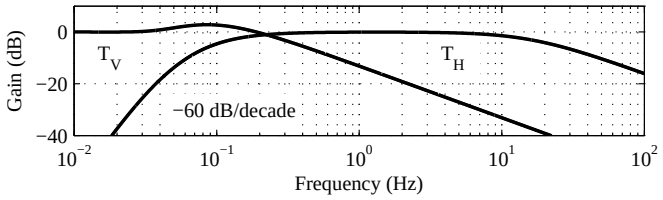

Fig. 9. Frequency responses of the closed loop transfers T_H and T_V, the voltage controller has a bandwidth of 0.5857 Hz

In order to design the power smoother for this particular case, the first step is to decide the cut-off frequency ω^d. It is clear from the spectrum of P_{ren} in Fig. 8 that ω^d is 6.91 rad/s (1.1 Hz). To attenuate the output power P_{out} in frequencies above ω^d, the magnitude of the frequency response of transfer function $T_H(s)$ should be one at 6.91 rad/s. To achieve this with a reasonable controller order, ω_c is set at 0.3462 rad/s. A power smoother of order 3 has proved to be sufficient to suppress the 1.1 Hz component without oversizing the supercapacitors for this particular application. The ESS rated power P_{ESD} is set at the 25 % of the nominal power of the renewable source, 100 kW. By applying equations (6)-(10), the required energy to generate the spectrum is 80.51 Wh. With the procedure described in section III-B a filter with the frequency response shown in Fig. 9 is synthesized. The bode plot in Fig. 9 shows the closed loop transfer functions T_V and T_H corresponding to the designed voltage controller.

A. Simulation results

The power smoother designed in the previous subsection is first evaluated by simulation. The scenario includes a wind turbine model generating the power profile shown in Fig. 8 connected to an AC network with a short circuit ratio of 2.5 (weak network). Power and supercapacitors voltage obtained by simulation can be seen in Fig. 10. The gray lines correspond to the power injected by the wind turbine P_{ren} (top plot) and the voltage reference V^*_{ESD} (bottom plot), respectively. The rest of lines correspond to the results obtained with a smoother controller of order one and three (dashed and solid lines, respectively). In the first seconds, in both cases, supercapacitors voltage V_{ESD} reaches the low voltage limit (250 V, in this example) due to the initial transient. Nevertheless, clearly the third order controller is more effective to regulate the

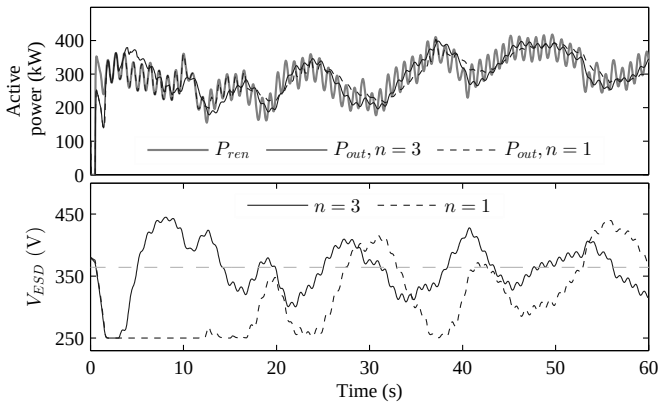

Fig. 10. Simulation results corresponding to the 3^{rd} order (solid black lines) and PI (dashed black lines) controllers with $\omega_c = 0.3462$ rad/s. The gray lines corresponds to P_{ren} in the top plot, and V^*_{ESD} in the bottom plot

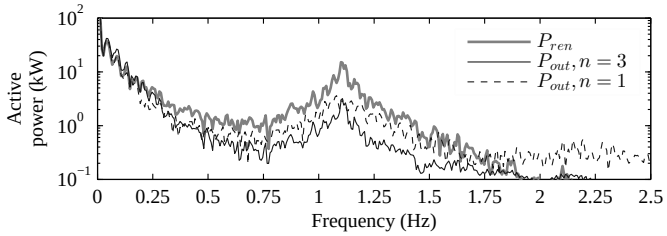

Fig. 11. Spectrum of P_{ren} and P_{out}, for the 3^{rd} and 2^{nd} order controllers, respectively

voltage than the simple PI. The better effectiveness of the third order controller can also be observed in the power smoothing. The PI power smoothing controller exhibits less attenuation in frequencies below ω^d than the third order controller. Such low attenuation causes larger deviations in the voltage reaching the limits in some points. In contrast, the third order controller is capable of blocking low frequencies, resulting in a smaller voltage variation. If a smoother output power P_{out} is needed, the filter parameter ω_c could be reduced, at the expense of a higher energy capacity required by the storage element.

Fig. 11 presents the frequency analysis of two simulations showing the differences between the two controllers. The resonance frequency of 1.1 Hz in P_{ren} has been effectively damped by both power smoothing controllers. Nevertheless, higher order controller is more capable of discerning the two control objectives. The attenuation at the frequency of 1.1 Hz is similar, although the PI controller exhibits more energy in the rest of the frequencies. This is translated in a more oscillating power as shown in Fig. 10. If such behavior is not acceptable for a particular application, a higher order filter should be used.

B. Experimental results

The power smoother is also evaluated experimentally. In this case, with the aim of obtaining a good resolution, the wind power profile in Fig. 8 is scaled to fit the emulator limits (± 4 kW in this case). As a consequence, the wind power profile used in the experiments has a mean value near zero. In

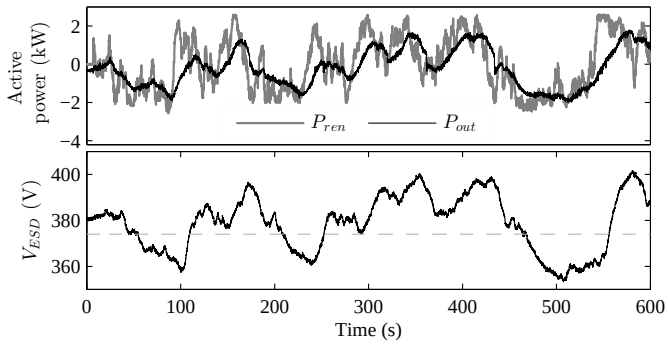

Fig. 12. Experimental results corresponding to a 3^{rd} order smoother controller with $\omega_c = 0.3462$ rad/s

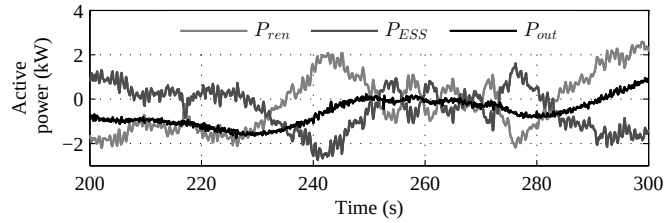

Fig. 13. Details of the three power of interest: P_{ren} (light gray), P_{ESS} (dark gray) and P_{out} (black), obtained with the experimental set-up

simulations, it has already been validated that the power filter is capable of smoothing a fluctuating generation with a mean power different from zero. The power smoother implemented in the experimental set-up has the same parameters than the simulated model to produce comparable results. In both cases, the capacity of filtering element is the same. Only the results of the third order controller are presented to avoid a long exposition.

The generated power P_{ren} with the resulting power P_{out} and the supercapacitor bank voltage V_{ESD} obtained in the experiments can be seen in Fig. 12. It is clear that the proposed smoothing scheme is able to achieve an effective attenuation of high frequency components in the power while maintain voltage close to the reference value. It must be noted that supercapcitors are oversized for this particular application, as in the available equipment, the rated power of both converters are close. As a consequence, the voltage magnitude could vary less than in a real application.

Fig. 13 presents a detail of the three power of interest: P_{ren}, P_{ESS} and P_{out}. This figure serves to show the cancellation of high frequency components of P_{ren}. Fast variations on the power P_{ren} can be observed (lighter line) being compensated by the power generated by the smoothing controller (dark gray) resulting in a smooth power output (black line).

The spectrum of P_{out} shown in Fig. 14 (black line) is the resulting smoothed power injected to the grid. It can be observed that the resonance at 1.1 Hz present in P_{ren} (gray line) is effectively damped in P_{out}. As a consequence of acquisition noise, the signals presented in Fig. 14 have more variability than its counterparts in Fig. 11.

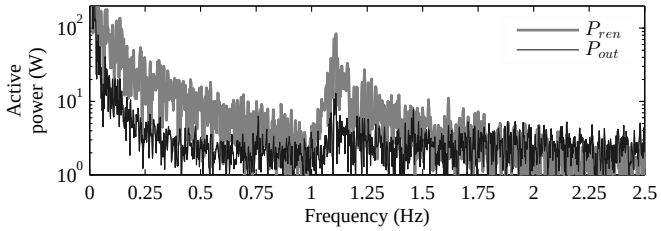

Fig. 14. Spectrum of P_{ren} and P_{out}, for the 3^{rd} and 2^{nd} order controllers, respectively

C. Discussion and comparison with previous results

The comparison of the proposed smoothing strategy with other previous results is difficult because of most of the other smoothing schemes use different storage technologies and topologies. A similar topology can be found in [17] but the storage device is a flywheel with a control scheme based on fuzzy control. Supercapacitors and flywheels are technologies in different power ranges. Supercapacitor systems are still not available for power ratings in the range of MW but it is a promising technology to be considered for power smoothing in smaller scale applications. To compare ESS for power smoothing, the ratio (MJ/MW) of energy of the ESS over rated power of the power source can be used; the lower the ratio the better. In [17] an ESS of 0.7 MW (approx. 19 MJ) is used for smoothing a 1.8 MW wind farm (1.1 MJ/MW). In this paper, a similar smoothed power is achieved with an ESS of 100 kW (approx. 0.28 MJ) with a wind turbine of 0.375 MW (0.75 MJ/MW). The proposed control scheme is also simpler of implementing than the one in [17]. In [11], the authors describe a wind power smoothing system based on supercapacatiors, with a different system topology and control scheme. The smoothing levels achieved in [11] are comparable to those obtained here. Nevertheless, the algorithm used in [11] is more sensitive to forecasting errors in contrast with the algorithm proposed in this article, which only uses past values of the generated power for filtering.

V. Conclusions

This paper has presented a power smoothing strategy based on supercapacitors for its application in weak AC networks or microgrids. The power smoothing strategy has been based on a voltage controller that manages the supercapacitors state of charge while at the same time generates a power profile capable of smoothing the varying power of renewable sources.

The proposed voltage controller has been aimed to simplify the implementation, even higher order than the presented in the case of study could be easily implemented in typical digital signal processor used in power converter. The design procedure has been reduced to a standard pole placement problem and guidelines for selecting the storage element have been provided. It is worth noticing the simplicity of the proposed scheme, since it only requires the design and implementation of a voltage controller for supercapacitors, besides the lower current loops, to smooth power injected by an arbitrary source.

REFERENCES

[1] R. Salim, M. Oleskovicz, and R. Ramos, "Power quality of distributed generation systems as affected by electromechanical oscillations definitions and possible solutions," *IET Generation, Transmission & Distribution*, vol. 5, no. 11, p. 1114, 2011.

[2] P. K. Ray, S. R. Mohanty, and N. Kishor, "Classification of Power Quality Disturbances Due to Environmental Characteristics in Distributed Generation System," *IEEE Trans. Sustainable Energy*, vol. 4, no. 2, pp. 302–313, Apr. 2013.

[3] M. Prodanovic and T. Green, "High-quality power generation through distributed control of a power park microgrid," *IEEE Trans. Ind. Electron.*, vol. 53, no. 5, pp. 1471–1482, 2006.

[4] M. Bollen and F. Hassan, *Integration of Distributed Generation in the Power System*. John Wiley & Sons Inc., Hoboken, New Jersey, 2011.

[5] "IEEE recommended practices and requirements for harmonic control in electrical power systems," *IEEE Std 519-1992*, p. section 10.5 Flicker, 1993.

[6] H. Geng, D. Xu, B. Wu, and G. Yang, "Active damping for pmsg-based wecs with dc-link current estimation," *IEEE Trans. Ind. Electron.*, vol. 58, no. 4, pp. 1110–1119, April 2011.

[7] F. Díaz-González, A. Sumper, O. Gomis-Bellmunt, and R. Villafáfila-Robles, "A review of energy storage technologies for wind power applications," *Renewable and Sustainable Energy Reviews*, vol. 16, no. 4, pp. 2154–2171, 2012.

[8] K. Kankanamge and N. Kularatna, "Improving the end-to-end efficiency of dc-dc converters based on a supercapacitor-assisted low-dropout regulator technique," *IEEE Trans. Ind. Electron.*, vol. 61, no. 1, pp. 223–230, 2014.

[9] R. Cardenas, R. Pena, G. Asher, and J. Clare, "Control strategies for enhanced power smoothing in wind energy systems using a flywheel driven by a vector-controlled induction machine," *IEEE Trans. Ind. Electron.*, vol. 48, no. 3, pp. 625–635, Jun. 2001.

[10] R. Cardenas, R. Pena, G. Asher, J. Clare, and R. Blasco-Gimenez, "Control strategies for power smoothing using a flywheel driven by a sensorless vector-controlled induction machine operating in a wide speed range," *IEEE Trans. Ind. Electron.*, vol. 51, no. 3, pp. 603–614, 2004.

[11] C. Abbey and G. Joos, "Supercapacitor Energy Storage for Wind Energy Applications," *IEEE Trans. Ind. Appl.*, vol. 43, no. 3, pp. 769–776, 2007.

[12] J. Aubry, P. Bydlowski, B. Multon, H. B. Ahmed, and B. Borgarino, "Energy Storage System Sizing for Smoothing Power Generation of Direct Wave Energy Converters," in *Proc. of the 3rd International Conference on Ocean Energy*, 2010, pp. 1–7.

[13] D. B. Murray, J. G. Hayes, D. L. O'Sullivan, and M. G. Egan, "Supercapacitor Testing for Power Smoothing in a Variable Speed Offshore Wave Energy Converter," *IEEE J. Ocean. Eng.*, vol. 37, no. 2, pp. 301–308, Apr. 2012.

[14] X. Liu, P. C. Loh, P. Wang, and F. Blaabjerg, "A direct power conversion topology for grid integration of hybrid ac/dc energy resources," *IEEE Trans. Ind. Electron.*, vol. 60, no. 12, pp. 5696–5707, 2013.

[15] M. E. Baran, S. Teleke, L. Anderson, A. Huang, S. Bhattacharya, and S. Atcitty, "STATCOM with energy storage for smoothing intermittent wind farm power," *Proc. of the Power and Energy Society General Meeting*, pp. 1–6, Jul. 2008.

[16] R. M. Kamel, A. Chaouachi, and K. Nagasaka, "Wind power smoothing using fuzzy logic pitch controller and energy capacitor system for improvement Micro-Grid performance in islanding mode," *Energy*, vol. 35, no. 5, pp. 2119–2129, May 2010.

[17] G. O. Suvire, M. G. Molina, and P. E. Mercado, "Improving the Integration of Wind Power Generation Into AC Microgrids Using Flywheel Energy Storage," *IEEE Trans. Smart Grid*, vol. 3, no. 4, pp. 1945–1954, Dec. 2012.

[18] J. Guerrero, P. C. Loh, T.-L. Lee, and M. Chandorkar, "Advanced control architectures for intelligent microgrids part ii: Power quality, energy storage, and ac/dc microgrids," *IEEE Trans. Ind. Electron.*, vol. 60, no. 4, pp. 1263–1270, 2013.

[19] K. Yoshimoto, T. Nanahara, and G. Koshimizu, "New Control Method for Regulating State-of- Charge of a Battery in Hybrid Wind Power/Battery Energy Storage System," in *Proc. of the PES Power Systems Conference and Exposition*. IEEE, 2006, pp. 1244–1251.

[20] S. Jayasinghe and D. Vilathgamuwa, "Flying supercapacitors as power smoothing elements in wind generation," *IEEE Trans. Ind. Electron.*, vol. 60, no. 7, pp. 2909–2918, 2013.

[21] F. Inthamoussou, J. Pegueroles-Queralt, and F. Bianchi, "Control of a supercapacitor energy storage system for microgrid applications," *IEEE Trans. Energy Convers.*, vol. 28, no. 3, pp. 690–697, 2013.

[22] F. D. Bianchi, A. Egea-Alvarez, A. Junyent-Ferr, and O. Gomis-Bellmunt, "Optimal control of voltage source converters under power system faults," *Control Engineering Practice*, vol. 20, pp. 539–546, 2012.

[23] A. Yazdani and R. Iravani, *Voltage-sourced converters in power systems*. Hoboken, New Jersey: John Wiley & Sons, Inc., 2010.

[24] C.-T. Chen, *Linear System Theory and Design*, 3rd ed. New York, NY, USA: Oxford University Press, Inc., 1998.

[25] a. Laub, M. Heath, C. Paige, and R. Ward, "Computation of system balancing transformations and other applications of simultaneous diagonalization algorithms," *IEEE Trans. Autom. Control*, vol. 32, no. 2, pp. 115–122, Feb. 1987.

[26] T. K. A. Brekken, A. Yokochi, A. von Jouanne, Z. Z. Yen, H. M. Hapke, and D. A. Halamay, "Optimal Energy Storage Sizing and Control for Wind Power Applications," *IEEE Trans. Sustainable Energy*, vol. 2, no. 1, pp. 69–77, Jan. 2010.

[27] A. Ruiz-Alvarez, A. Colet-Subirachs, F. Alvarez-Cuevas Figuerola, O. Gomis-Bellmunt, and A. Sudria-Andreu, "Operation of a utility connected microgrid using an iec 61850-based multi-level management system," *IEEE Trans. Smart Grid*, vol. 3, no. 2, pp. 858–865, 2012.

[28] C. Nichita, D. Luca, B. Dakyo, and E. Ceanga, "Large band simulation of the wind speed for real time wind turbine simulators," *IEEE Trans. Energy Convers.*, vol. 17, no. 4, pp. 523–529, Dec. 2002.

[29] T. Petru and T. Thiringer, "Modeling of wind turbines for power system studies," *IEEE Trans. Power Syst.*, vol. 17, no. 4, pp. 1132–1139, Nov. 2002.

[30] T. Thringer and J.-A. Dahlberg, "Periodic pulsations from a three-bladed wind turbine," *IEEE Trans. Energy Convers.*, vol. 16, no. 2, pp. 128–133, Jun. 2001.

Jordi Pegueroles-Queralt was born in Barcelona, Catalunya in 1987. He received the M.Sc. degree in Engineering from the School of Industrial Engineering of Barcelona (ETSEIB), Technical University of Catalunya (UPC), Barcelona, Spain, in 2011, with the Master's Thesis given by the Politecnico di Torino, Italy. He was with the Humanoid-Lab group at the Institut de Robòtica i Informàtica Industrial from 2007 to 2011. From 2011 he is pursuing a Ph.D. degree at Catalonia Institute for Energy Research, Spain. His research interests are control theory applied to power electronics and renewable power sources.

F.D. Bianchi received the B.S. and Ph.D. degrees in electronic engineering from the National University of La Plata (UNLP), Argentina, in 1999 and in 2005, respectively. From 1999 to 2006, he was a Ph.D. student and a Postdoctoral Fellow at the Laboratory of Industrial Electronic, Control and Instrumentation (LEICI, UNLP, La Plata, Argentina). From 2006 to 2010, he was a Postdoctoral Researcher at the Technical University of Catalonia, Barcelona, Spain. In 2010, he joined the Power Electronics and Electric Power Grids Group, Catalonia Institute for Energy Research (IREC), Barcelona, as a Scientific Researcher. His main research interests include robust control and linear parameter-varying systems and their applications to the control of renewable energy conversion systems.

Oriol Gomis-Bellmunt (S'05-M'07-SM'12) received the degree in industrial engineering from the School of Industrial Engineering of Barcelona (ETSEIB), Technical University of Catalonia (UPC), Barcelona, Spain, in 2001 and the PhD in electrical engineering from the UPC in 2007. In 1999 he joined Engitrol S.L. where he worked as project engineer in the automation and control industry. In 2003 he developed part of his PhD thesis in the DLR (German Aerospace center) in Braunschweig (Germany). Since 2004 he is with the Electrical Engineering Department of the UPC where he is lecturer and participates in the CITCEA-UPC research group. Since 2009 he is also with the Catalonia Institute for Energy Research (IREC). He is member of the editorial board of IEEE Transactions on Power Delivery, for HVDC and integration of wind power in power systems. His research interests include the fields linked with smart actuators, electrical machines, power electronics, renewable energy integration in power systems, industrial automation and engineering education.